

Measurement of viscoelastic properties of homogeneous soft solid using transient elastography: An inverse problem approach

S. Catheline,^{a)} J.-L. Gennisson, G. Delon, M. Fink, R. Sinkus,^{b)} S. Abouelkaram,^{c)} and J. Culioli^{c)}

Laboratoire Ondes et Acoustique, ESPCI, Université Paris VII, U.M.R. C.N.R.S. 7587, 10 rue Vauquelin, 75231 Paris cedex 05, France

(Received 2 February 2004; revised 1 September 2004; accepted 20 September 2004)

Two main questions are at the center of this paper. The first one concerns the choice of a rheological model in the frequency range of transient elastography, sonoelasticity or NMR elastography for soft solids (20–1000 Hz). Transient elastography experiments based on plane shear waves that propagate in an Agar-gelatin phantom or in bovine muscles enable one to quantify their viscoelastic properties. The comparison of these experimental results to the prediction of the two simplest rheological models indicate clearly that Voigt's model is the better. The second question studied in the paper deals with the feasibility of quantitative viscosity mapping using inverse problem algorithm. In the ideal situation where plane shear waves propagate in a sample, a simple inverse problem based on the Helmholtz equation correctly retrieves both elasticity and viscosity. In a more realistic situation with nonplane shear waves, this simple approach fails. Nevertheless, it is shown that quantitative viscosity mapping is still possible if one uses an appropriate inverse problem that fully takes into account diffraction in solids. © 2004 Acoustical Society of America. [DOI: 10.1121/1.1815075]

PACS numbers: 43.80.Vj, 43.80.Ev, 43.20.Qf [Fd]

Pages: 3734–3741

I. INTRODUCTION

Elasticity mapping is an effective method for detecting tumors in soft tissues. Images of elasticity can be achieved with static elastography¹ or dynamic elastography (sonoelasticity,^{2,3} NMR elastography,^{4,5} or transient elastography^{6,7}). The dynamic methods present the advantage of potentially revealing the medium dynamic properties^{8,9} such as viscosity. In the simple case of a plane monochromatic shear wave for example, the speed and attenuation are deduced from the phase and amplitude measurements, which can be converted into elasticity and viscosity. This last computational step requires choosing an appropriate rheological model. The simplest viscoelastic models (utilizing two parameters) are Voigt's model and Maxwell's model. Although the first one is more often used for solids and the second one for liquids, the choice is not obvious in liquid-like solids such as soft tissues since both models are used in the literature.^{10–12} Moreover, in the dynamic elastography frequency range (20–1000 Hz), no commercially available rheometer exists (typically 0.01–10 Hz). Homemade rheometers moreover tend to present resonance and propagation difficulties.^{13,14} This paper may contribute to fill this gap in experimental data.

II. EXPERIMENT

In our experimental study, we used an ultrafast ultrasonic scanner.^{15,16} It provides images of the echogenicity of tissues similar to a standard echographic device but with a

rate of 5000 frames/s (about 100 times higher than conventional scanners). It includes a medical ultrasonic array with 128 channels working at 5 MHz. Each channel is connected to a 2 Mbytes memory, the echoes are sampled at 50 MHz and digitized with 9 bit resolution. In a typical experiment, 250 echographic images are recorded in memory with a cadence of 3000 frames/s. A movie of the displacement is obtained using correlation algorithms between successive speckle images. Thus, it allows one to detect fast tissue motion induced by low frequency shear waves inside the medium. The apparatus can measure displacements as small¹⁷ as 1 μm . As shown in Fig. 1, the low frequency (50–500 Hz) shear wave is generated by transversally shaking a rigid aluminum plate (110 \times 170 mm²) applied on one side of the phantom with a vibrator (Bruel&Kjaer 4810 type). The phantom is a mixture of water with 3% gelatin and 2% agar. The transverse displacement field of the shear wave is measured in a plane perpendicular to the rigid plate (40 \times 40 mm²). The displacement field, displayed in Fig. 2, confirms the plane nature of the shear wave. The 100 Hz shear wave propagates from bottom to top in the four sequential images selected from the displacement field movie. The use of such plane waves simplifies the analysis of the viscoelastic properties of soft solids since viscoelastic theories often utilize this assumption. From the displacement field along the axis of the rigid plate ($z=20$ mm), Fig. 3(a), the phase and the amplitude as a function of depth are computed, Figs. 3(b) and 3(c). The speed, $C_T=2.26\pm 0.003$ m s⁻¹, and the attenuation, $\alpha_T=23\pm 1$ m⁻¹, are then deduced. The experimental errors are estimated from the linear fit deviations. We point out that the estimate of the phase slope as a function of depth is less subjected to noise than the amplitude slope. Consequently, attenuation measurements may be difficult in noisy situations. The experiment is repeated for frequencies rang-

^{a)}Electronic mail: stefan.catheline@espci.fr

^{b)}Also at: Philips Research Laboratories, Division Technical System, Röntgenstrasse 24-26, D-22335, Hamburg, Germany.

^{c)}Also at: Station de Recherches sur la Viande, INRA, Theix, 63122 St Genès Champanelle, France.

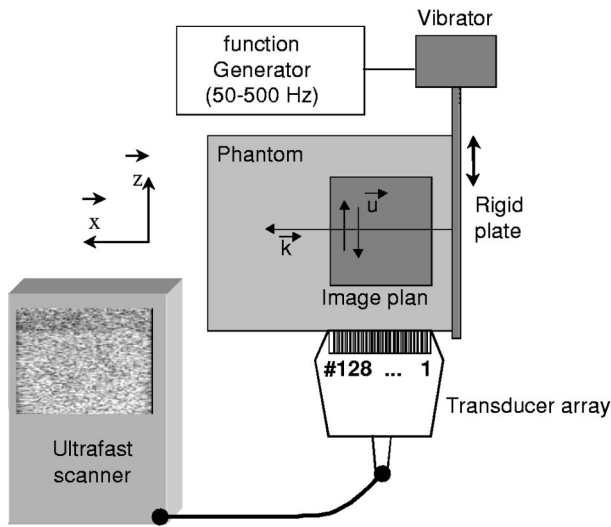


FIG. 1. Experimental setup. A low frequency plane shear wave is generated in an Agar-gelatin phantom by shaking a rigid plate with a vibrator. The wave propagates along the direction \mathbf{k} . In the meantime, a medical transducer array, connected to an ultrafast scanner, insonifies the medium on a $40 \times 40 \text{ mm}^2$ area (gray area). Then a correlation algorithm, on speckle images stored in memory, computes the displacement field \mathbf{u} within the phantom.

ing from 50 to 500 Hz with a 25 Hz step. The shear wave measurements as a function of the central frequency, Fig. 4 (circles), show a rather flat speed distribution and a strongly varying attenuation distribution (from 5 to 80 m^{-1}). The maximum error occurs at 500 Hz, because the amplitude of the shear wave drops with the increase in frequency: $\Delta C_T = 0.007 \text{ m s}^{-1}$ and $\Delta \alpha_T = 4 \text{ m}^{-1}$. This reliable experimental data will be the reference measurements in the following.

III. THE INVERSE PROBLEM APPROACH

The elasticity mapping in transient elastography is performed with some inverse problem algorithm. We propose

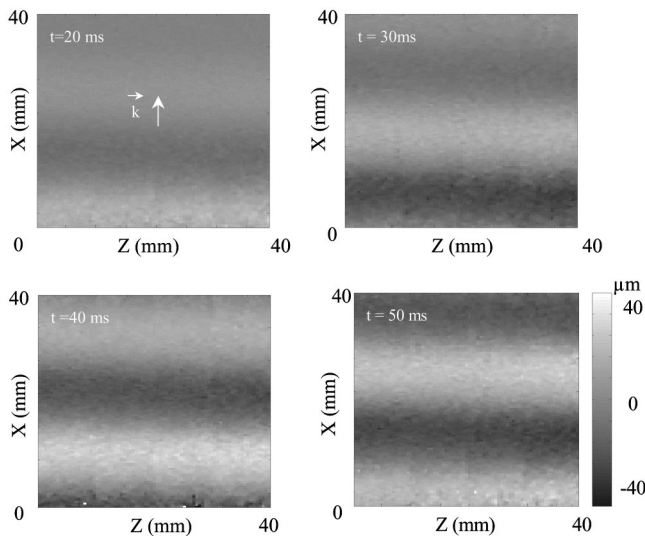


FIG. 2. Typical experimental transverse displacement field (z component) of a 100 Hz shear wave. These images are extracted from a movie at different acquisition times 20, 30, 40, 50 ms after a few cycles of sinusoid are generated from the bottom of the images. The arrow indicates the direction of propagation \mathbf{k} . The plane property of the shear wave is clearly visible: it is a transverse wave.

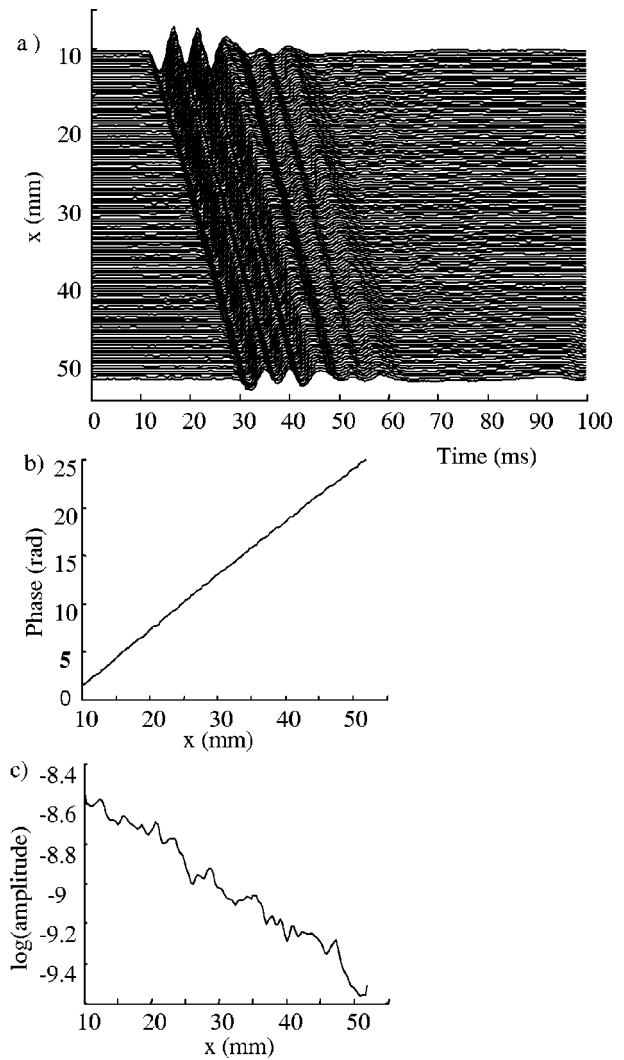


FIG. 3. (a) Seismic representation of the transverse displacement field. (b) The phase and (c) the amplitude are computed from a spectral analysis at the central frequency 100 Hz. Linear fits give the speed ($C_T = 2.265 \pm 0.003 \text{ m s}^{-1}$) and the attenuation ($\alpha_T = 23 \pm 1 \text{ m}^{-1}$).

here a very simple one to measure both the local elasticity and viscosity. In the simple case of a plane monochromatic shear wave, the starting point is the one-dimensional (1D) Helmholtz equation:

$$\frac{\partial^2 \text{FT}_t(u_z(x))}{\partial x^2} + k^2 \text{FT}_t(u_z(x)) = 0, \quad (1)$$

where FT_t , u_z , and x stand for the time Fourier transform, the transverse displacement, and the longitudinal coordinate, respectively. Thus the local complex wave vector is given by

$$k = \sqrt{\frac{\partial^2 \text{FT}_t(u_z(x))}{\partial x^2} / \text{FT}_t(u_z(x))}, \quad (2)$$

and the local speed C_T and attenuation α_T are expressed as

$$C_T = \frac{\omega}{\text{Re}\{k\}}, \quad \alpha_T = \text{Im}\{k\}. \quad (3)$$

Thus, the latter set of equations constitute the basis of an algorithm that permits one to compute the local speed and

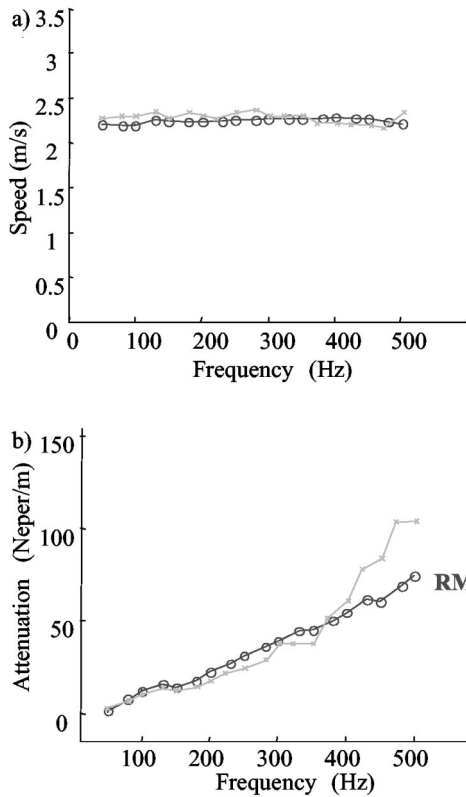


FIG. 4. Speed and attenuation measurements of the transverse wave as a function of the frequency. (a) The inverse problem algorithm gives a good estimation of speed (crosses) compared to the reference measurement obtained with a spectral analysis of the displacement field method (more reliable but nonlocal). (b) However the inverse problem approach for attenuation measurements seems to be more sensitive to noise since a deviation from the reference measurements (circles) is visible beyond 400 Hz.

the local attenuation from the local displacement field $u_z(x)$. Its application to a homogeneous Agar-gelatin based phantom serves to test the feasibility of the technique in a very simple configuration. The results obtained from the inverse problem algorithm and those obtained from the phase and amplitude, Fig. 4 (cross), are very close: within 5% for the speed and within 11% for the attenuation below 400 Hz. The deviation in the reconstructed values of attenuation above 400 Hz is due to a poor signal-to-noise ratio in displacement. Thus, not only is the speed correctly recovered using the inverse problem algorithm, which has already been demonstrated,¹⁸ but also attenuation even though it is more sensitive to noise. As a consequence, viscosity mapping should be possible if a suitable rheological model is chosen.

IV. VOIGT'S VERSUS MAXWELL'S MODEL

At a given frequency, two experimental measurements of phase and amplitude allow one to compute the local speed and attenuation, from which the elasticity and viscosity estimates are deduced. This last step requires a rheological model. These viscoelastic models, which require only two parameters, are Voigt (V) and Maxwell's (M) models, Fig. 5. Both models are composed of a dashpot and a spring, but they are placed in parallel (V) or in series (M) depending on the model. The stress-strain relationships are, respectively,

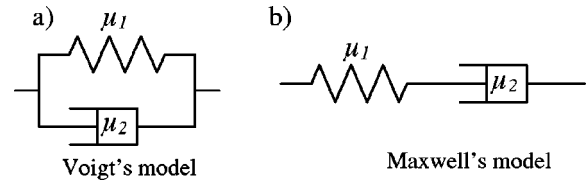


FIG. 5. (a) The Voigt's model is composed of a spring, with spring constant μ_1 , and a dashpot, with coefficient of viscosity μ_2 , in parallel. (b) The Maxwell's model is a spring and a dashpot in series.

$$\sigma = \left(\mu_1 - \mu_2 \frac{\partial}{\partial t} \right) \varepsilon, \quad \left(\mu_1 + \mu_2 \frac{\partial}{\partial t} \right) \sigma = \mu_1 \mu_2 \frac{\partial \varepsilon}{\partial t}. \quad (4)$$

The stress σ is linked to the strain ε via the shear elasticity μ_1 , the shear viscosity μ_2 , and the time-derivative operator $\partial/\partial t$. Inserting these relations for monochromatic excitation into the equation of motion, one obtains the 1D Helmholtz equation for Voigt's model and Maxwell's model, respectively,

$$\frac{\partial^2 U}{\partial x^2} + \frac{\rho \omega^2}{(\mu_1 + i \omega \mu_2)} U = 0, \quad (5)$$

$$\frac{\partial^2 U}{\partial x^2} + \frac{\rho \omega^2 (\mu_1 + i \omega \mu_2)}{i \omega \mu_1 \mu_2} U = 0,$$

where ρ is the density and U the Fourier transform of the displacement. Then, from the complex wave vector, the transverse wave speed (C_T^V, C_T^M) as well as the attenuation (α_T^V, α_T^M) can be computed for each model:

$$C_T^V = \sqrt{\frac{2(\mu_1^2 + \omega^2 \mu_2^2)}{\rho(\mu_1 + \sqrt{\mu_1^2 + \omega^2 \mu_2^2})}}, \quad (6)$$

$$C_T^M = \sqrt{\frac{2\mu_1}{\rho \left(1 + \sqrt{1 + \frac{\mu_1^2}{\omega^2 \mu_2^2}} \right)}},$$

$$\alpha_T^V = \sqrt{\frac{\rho \omega^2 (\sqrt{\mu_1^2 + \omega^2 \mu_2^2} - \mu_1)}{2(\mu_1^2 + \omega^2 \mu_2^2)}}, \quad (7)$$

$$\alpha_T^M = \sqrt{\frac{\rho \omega^2 \left(\sqrt{1 + \frac{\mu_1^2}{\omega^2 \mu_2^2}} - 1 \right)}{2\mu_1}}.$$

In order to compare the theoretical predictions of Voigt and Maxwell's models to the experimental data, one frequency is chosen arbitrarily, for example, 400 Hz. With the measured values of Fig. 6, $C_T(400) = 2.282 \pm 0.004 \text{ m s}^{-1}$ and $\alpha_T(400) = 54 \pm 1 \text{ m}^{-1}$, it is possible to evaluate μ_1 and μ_2 using Eqs. (6) and (7). Voigt's model gives $\mu_1 = 5.67 \pm 0.02 \text{ kPa}$ and $\mu_2 = 0.22 \pm 0.01 \text{ Pa s}$ and Maxwell's model $\mu_1 = 5.73 \pm 0.02 \text{ kPa}$ and $\mu_2 = 23 \pm 1 \text{ Pa s}$. Both models provide similar values for the elasticity. However, there is a difference of two orders of magnitude for the viscosity. In the literature, the viscosity for gelatin rarely exceeds 1 Pa s. For example, with Zener's model in gelatin at 1.5 Hz, Djajburov *et al.*¹⁹ found 0.21 Pa s, very close to the value ob-

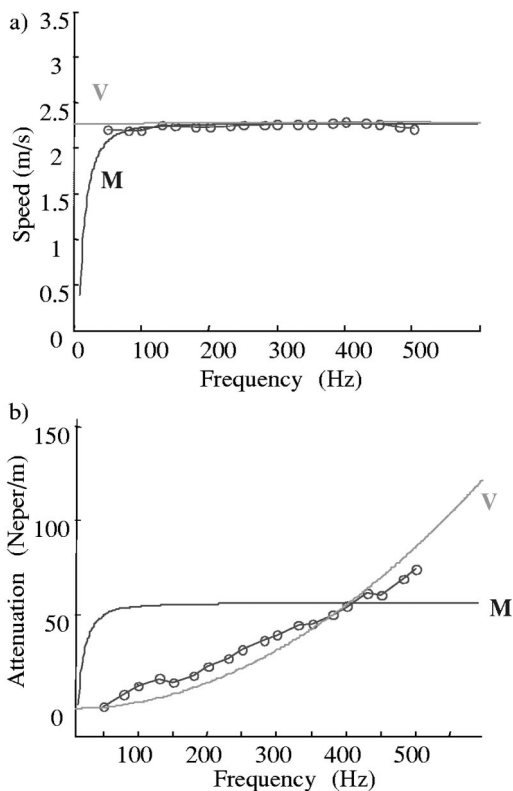


FIG. 6. Transverse wave speed and attenuation measurements vs frequency. (a) The flat speed distribution (circles) is correctly predicted by the Voigt's (V) and the Maxwell's model (M). (b) On the other hand, the Maxwell's model attenuation predictions cannot properly account for the experimental distribution (circles). Voigt's model is better.

tained with the Voigt's model. This result indicates that Voigt's model seems to be more appropriate for the description of viscous effects in case of the Agar-gelatin phantom. Now, a study of the prediction of each model for all the other frequencies reveals that both models are correct as far as the speed is concerned, Fig. 6(a). The dispersion curve of the speed, therefore, does not allow for differentiating between the two models. On the other hand, the curve of attenuation versus frequency indicates a dramatic difference between Voigt and Maxwell's models and thus allows one to distinguish the good model: Voigt's model. Although this model is not perfect, it gives much better predictions for attenuation than Maxwell's model. The same general behavior is observed independent of the frequency chosen to fit the experimental data: an increasing law as ω^2 for Voigt's model and a plateau for Maxwell's model. Indeed, for frequencies beyond 100 Hz, the dashpot becomes "harder" than the spring. When these two elements are placed in series, as in Maxwell's model Fig. 5(b), the viscoelastic properties are entirely driven by the spring. Thus the speed and attenuation no longer depend on frequency: they present a plateau. Now, no plateau is reached in the measured attenuation curve, Fig. 6(b). As a result, the conclusion so far is that for Agar-gelatin based phantom, the best of the simplest rheological models is Voigt's model.

V. EXCISED POSTRIGOR BEEF MUSCLE

The next step is to conduct the plane shear wave experiment in real soft tissues. We have chosen an *excised post*

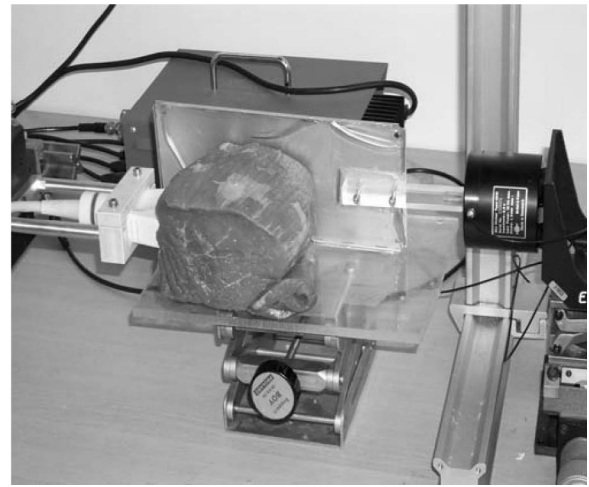


FIG. 7. Picture of the experimental setup in a beef muscle (*biceps femoris*). The vibrator transmits longitudinal oscillations to a rigid plate applied on the back side of the muscle sample. The transverse wave propagates in the direction of the fibers. The displacements are detected with a medical transducer array placed on the left-hand side of the muscle sample and connected to an ultrafast scanner.

rigor beef muscle: the *biceps femoris*. Figure 7 shows, from right to left, the vibrator, the duralumin rigid plate applied on the back face of the muscle sample, and the transducer array applied on the left side of the sample. When shaken, the plate transmits low frequency vibrations as transverse waves with a polarization perpendicular to the fibers in this situation. The displacements are detected using the transducer array connected to the ultrafast scanner. The speed and the attenuation are represented in Fig. 8 as functions of frequency which ranges from 50 to 350 Hz. The reason why the fre-

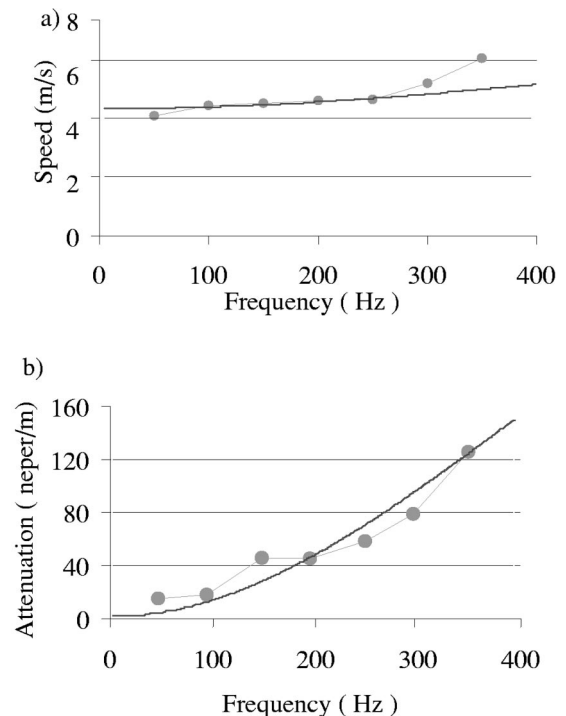


FIG. 8. Speed and attenuation vs frequency in a beef muscle. The transverse wave has a polarization perpendicular to the fibers. Theoretical predictions (solid lines) are based on a Voigt's model.

quency range ends at 350 Hz is that the attenuation ($\alpha \approx 80 \text{ m}^{-1}$ at 300 Hz) is approximately twice as large as in the Agar-gelatin based phantom ($\alpha \approx 40 \text{ m}^{-1}$ at 300 Hz) and thus the displacements are too small to be exploited until 500 Hz. Nevertheless, it is clear that these data are once again well described by Voigt's model since no plateau is present in the attenuation curve, Fig. 8(b). In addition, the biceps femoris muscle presents a transverse isotropy. General theoretical considerations on anisotropic viscoelastic media^{20,21} show that two shear elasticities and two shear viscosities are needed to properly describe the transverse isotropy. It should be noted that these theories generalize Hooke's law by adding a Newtonian viscous term in the stress tensor T_{ij} . Thus, the implicit viscoelastic model is Voigt's solid,

$$T_{ij} = c_{ijkl} S_{kl} + \eta_{ijkl} \frac{\partial S_{kl}}{\partial t}, \quad (8)$$

with c_{ijkl} denoting Christoffel's tensor, S_{kl} the strain tensor, and η_{ijkl} the viscosity tensor.

A slow and a fast wave are found depending on the polarization with respect to the fibers. Two elasticities and two viscosities are then deduced: $\mu_1^\perp = 25 \pm 1 \text{ kPa}$, $\mu_2^\perp = 3.3 \pm 0.4 \text{ Pa s}$, $\mu_1^\parallel = 49 \pm 2 \text{ kPa}$, $\mu_2^\parallel = 15 \pm 2 \text{ Pa s}$.

Thus the experimental measurements obtained with the plane shear wave experiment are in good agreement with previous work on muscles.^{22,23} In other soft bovine tissues such as calfskin, liver, or cardiac muscle, Voigt's model was shown to give fair predictions of ultrasonic shear wave speed and attenuation.²⁴

VI. THE 1D SHEAR ELASTICITY PROBE

The plane shear wave experiments presented in the first part of this paper can hardly be applied in real *in vivo* soft tissues. So what results can one expect from the inverse problem algorithm in a more realistic situation with nonplane shear waves?

We used the 1D shear elasticity probe.^{25,26} As shown in Fig. 9(a), the shear elasticity probe is composed of a single ultrasonic transducer mounted on a vibrator. It has the advantage of using simple electronics while giving a quantitative global estimate of elasticity. It can potentially be applied to the diagnosis of liver diseases.²⁷ In the following experiments, the same phantom as in the first part was tested with the shear elasticity probe. The shear wave is generated by the front face of the transducer meanwhile working in a pulse echo mode. The central frequency of the 7-mm-diam transducer is 5 MHz. Its focal is 35 mm. A scans are recorded in a 9 bit digitizer at a sampling frequency of 50 MHz. The repetition frequency between successive A-scans is fixed in the experiments at 3000 Hz. The longitudinal component of the displacement along the ultrasonic beam is computed using correlation algorithms. The complex diffraction pattern of a low frequency vibrator,²⁸ assures that we are not working with plane shear waves. A typical experimental displacement field is shown in Fig. 9(b). When a 100 Hz central frequency pulse is applied, a fast compression wave (P), a slow shear wave (S), as well as a reflected shear wave from the bottom of the sample are visible. If the same algorithm

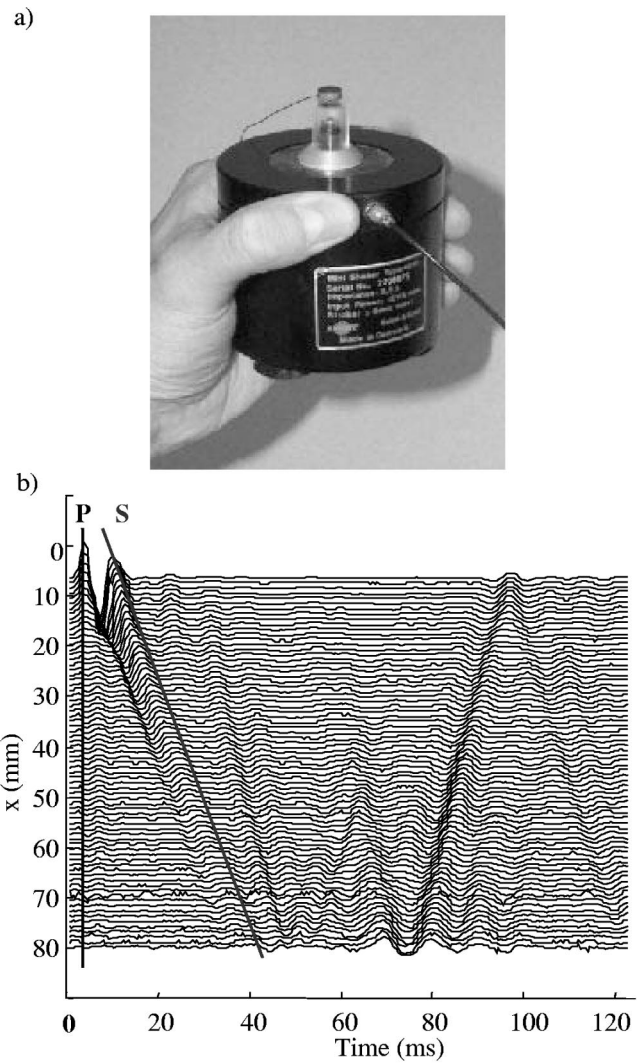


FIG. 9. (a) Picture of the 1D shear elasticity probe. A single ultrasonic transducer is mounted on a vibrator. (b) Seismic representation of the longitudinal component (along the x axis) of the displacement field. A compression (P), a shear (S), and a reflected shear waves are visible when a 100 Hz central frequency pulse is applied from the top ($x=0$) of an Agar-gelatin based phantom.

used for plane shear waves is directly applied to the latter measurements, a very good speed estimate is obtained, Fig. 11(a). Nevertheless, the attenuation is overestimated, Fig. 11(b). The reasons for this apparent overattenuation must be found in the inverse problem algorithm. In order to carefully study the underlying approximations of the algorithm, one can start with the most general wave equation in an isotropic and linear solid, Eq. (8). For the sake of simplicity, the medium is considered as purely elastic. Adding viscosity does not change the essential argument:

$$(\lambda + 2\mu) \nabla \nabla \mathbf{u} + \mu \nabla^2 \mathbf{u} - \rho \frac{\partial^2 \mathbf{u}}{\partial t^2} = \mathbf{0}. \quad (9)$$

The first assumption one needs in order to obtain the Helmholtz equation used in the inverse problem algorithm is that the compression term, the first one in Eq. (9), is negligible. It is referred to as the compression-free approximation (also called the Helmholtz approximation). In order to justify this assumption, one notes that it is possible to clearly separate

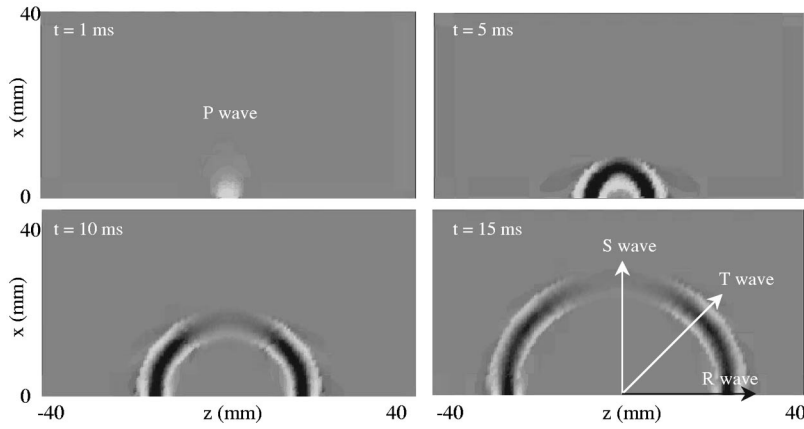


FIG. 10. Simulation of the displacement field using the exact Green's functions in a semi-infinite elastic solid. A pulse is applied from the bottom by a 7 mm circular piston source. At $t = 1$ ms, the compression wave is visible. Then the shear wave propagates as a Rayleigh wave (R) at the surface, as a transverse wave (T) in the oblique direction and as a near field shear wave (S) in the axis of the piston.

the displacement induced by the compression wave and that induced by the shear wave in homogeneous media with transient elastography, Fig. 9(b). Nevertheless, getting rid of the compression wave is not so obvious as we shall see, especially in the usual experimental situation where waves are in the near field. The problem has thus been greatly simplified. The components of the displacement field u_i are decoupled and obey the same wave equation,

$$\mu \Delta u_i - \rho \frac{\partial^2 u_i}{\partial t^2} = 0, \quad i = x, y, z. \quad (10)$$

Since it is the only one measured experimentally, the x component is selected. Then the Laplacian operator reads:

$$\Delta u_x = \frac{\partial^2 u_x}{\partial x^2} + \frac{\partial^2 u_x}{\partial y^2} + \frac{\partial^2 u_x}{\partial z^2}. \quad (11)$$

One last simplification is needed. Indeed, the experimental configuration using the 1D shear elasticity probe allows measurement of only one component of the displacement in one dimension along the ultrasonic beam. The experiment requires us to neglect two terms in the Laplacian operator:

$$\frac{\partial^2 u_x}{\partial x^2} \gg \frac{\partial^2 u_x}{\partial y^2} + \frac{\partial^2 u_x}{\partial z^2}. \quad (12)$$

This second assumption is referred as the quasiplane approximation. Then, from the 1D wave equation,

$$\frac{\partial^2 u_x}{\partial x^2} - \frac{\rho}{\mu} \frac{\partial^2 u_x}{\partial t^2} = 0, \quad (13)$$

the Helmholtz equation is finally deduced for the case of monochromatic excitation:

$$\frac{\partial^2 u_x}{\partial x^2} + k^2 u_x = 0. \quad (14)$$

Consequently, what is a perfect inverse problem for (plane) transverse waves is only an approximate inverse problem for general diffracted shear waves (although well founded as far as speed measurements are concerned). So how can one compensate for the lack of information resulting from the compression-free and the quasiplane approximations? We used the analytical solution of the displacement field in a semi-infinite elastic solid induced by a point source applied perpendicularly to the surface.^{29,30} The theoretical longitudinal component (x component) of the displacement

field is represented on gray scale images, Fig. 10, after a 100 Hz central frequency pulse is applied from the bottom. One can distinguish a Rayleigh wave on the surface (R), a transverse wave (T) at 45° , and a shear wave along the axis of the source. The latter wave is precisely the one detected in the experiments using the 1D shear elasticity probe. If the inverse problem algorithm is applied to the theoretical longitudinal displacement in one dimension along the source axis just as in the experiment, one obtains a good estimation of the speed and a surprising (at first sight) nonzero attenuation even though the medium is ideally lossless, Fig. 11(b)

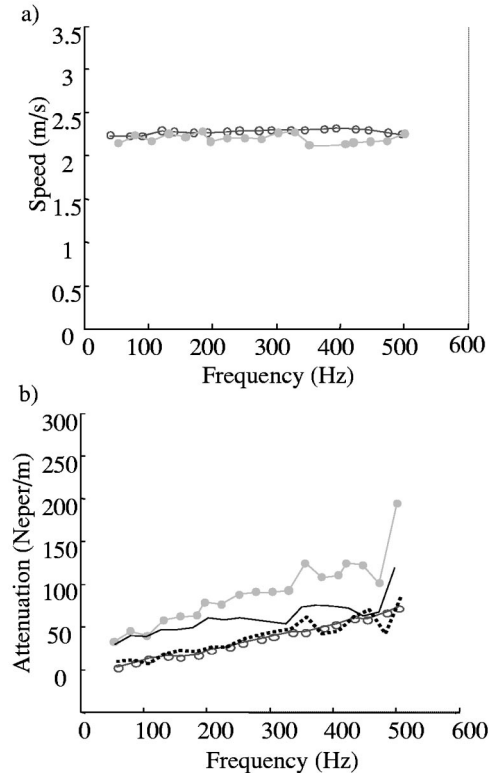


FIG. 11. Speed and attenuation measurements vs frequency. (a) The inverse problem speed estimation (dots) is very close (within 8%) to the reference measurements (circle). (b) But an overattenuation is clearly visible with the inverse problem method (dots) compared to the reference measurements (circle). Applied to the simulated data in a perfectly elastic solid, the inverse problem gives an overattenuation as well (solid line). Subtracting these latter data from the experimental measurements (dots) compensates for diffraction effects and allows one to compute the medium attenuation (dotted line).

(solid line). This paradox is a consequence of the approximations in the inverse problem. Indeed, diffraction, is seen by the inverse problem algorithm as a dissipative effect. It therefore computes an apparent attenuation due in reality to diffraction. Thus if one subtracts this apparent attenuation from the experimental measurements, the diffraction effects are eliminated and what remains is the attenuation due to the medium, Fig. 11(b) (dotted line). Consequently, speed and attenuation (or elasticity and viscosity) can be easily measured with the shear elasticity probe.

VII. DISCUSSION

Thus the Green's function simulation allows one to avoid bias due to diffraction. Another benefit of simulation is that the compression-free and quasiplane approximations, used in the inverse problem algorithm, can be tested. Surprisingly, it appears that the quasiplane approximation is very well founded since the left term of Eq. (12) is at least ten times bigger than the right-hand side terms in the experimental configuration.³¹ This ratio increases for the displacements measured farther and farther away from the source. Thus the Laplacian operator is correctly evaluated and the conclusion is that the main flaw in the approximated inverse problem algorithm comes from the first approximation, namely the compression-free approximation. Should not it be eliminated? The divergence of the displacement is almost zero and yet it would be a mistake to ignore the whole compression term. It would be ignoring the huge coefficient ($\lambda + 2\mu$) in front that makes the whole compression term non-negligible: the longitudinal wave is clearly visible, Fig. 9. The problem in a quasi-incompressible medium such as tissues is that no experimental devices (using ultrasounds or NMR) has the accuracy to experimentally evaluate this compression term. It should be noted that for the same reason, any Poisson's ratio mapping is not feasible with elastography except in the special case of porous soft materials.³² Nevertheless, as long as one is interested in phase (or speed) measurements, the compression-free approximation is valid. But it fails in amplitude (or attenuation) estimations and introduces important biases.

We have presented an experimental situation in which a single transducer is as good as a transducer array or a NMR device. A compression-free inverse problem algorithm does not lead to the correct value of attenuation along the axis of a point source. From a more general point of view, this experiment reveals that in order to correctly reconstruct the attenuation map (and thus a viscosity map), one has to fully take into account diffraction effects. It means that the inverse problem must follow from the exact wave equation, Eq. (9). So how can one reconcile the experimental limitation (the compression term cannot be evaluated) with the theoretical requirement (the exact wave equation has to be taken into account)? As shown previously in the simple case of a homogeneous medium, a first answer would be to use simulation. For heterogeneous media, the question is still open. A feasible exact inverse problem³³ is still needed in order to create a quantitative viscosity image.

VIII. CONCLUSION

Through a transient elastography experiment using plane shear waves in soft solids, this paper presents a simple inverse problem algorithm to estimate the speed and the attenuation. Moreover, it is demonstrated that the best of the simplest rheological model for an Agar-gelatin based phantom and a beef muscle sample is Voigt's solid. The conclusion of this first part is that quantitative viscosity can be retrieved from an inverse problem algorithm. Some difficulties remain in the more general case where nonplane shear waves are used. This is the subject of the second part. A simulation based on theoretical Green's function is shown to properly compensate for diffraction biases. Thus, a quantitative estimate of shear elasticity and shear viscosity is obtained with the so-called 1D shear elasticity probe in a homogeneous soft solid (Agar-gelatin phantom). For viscosity imaging (in heterogeneous media), diffraction effects require one to solve an exact inverse problem whose solution is yet to be imagined.

¹B. S. Garra, E. I. Cespedes, J. Ophir, S. R. Spratt, and R. A. Zuurbier, "Elastography of breast lesions: Initial clinical results," *Radiology* **202**, 79–86 (1997).

²S. F. Levinson, M. Shinagawa, and T. Sato, "Sonoelastic determination of human skeletal muscle elasticity," *J. Biomech.* **28**, 1145–1154 (1995).

³F. Lee, J. P. Bronson, R. M. Lerner, K. J. Parker, S. R. Huang, and D. J. Roach, "Sonoelasticity Imaging: Results in In vitro tissue specimens," *Radiology* **181**, 237–239 (1991).

⁴R. Muthupillari, D. J. Lomas, P. J. Rossman, J. F. Greenleaf, A. Manduca, and R. L. Ehman, "Magnetic resonance elastography by direct visualization of propagating acoustic strain wave," *Science* **269**, 1854–1857 (1995).

⁵D. B. Plewes, I. Betty, S. N. Urchuk, and I. Soutar, "Visualizing tissue compliance with MR imaging," *J. Magn. Reson. Imaging* **5**, 733–738 (1995).

⁶S. Catheline, F. Wu, and M. Fink, "A solution to diffraction biases in sonoelasticity: The acoustic impulse technique," *J. Acoust. Soc. Am.* **105**, 2941–2950 (1999).

⁷L. Sandrin, M. Tanter, S. Catheline, and M. Fink, "Shear modulus imaging with 2-D transient elastography," *IEEE Trans. Ultrason. Ferroelectr. Freq. Control* **49**, 426–435 (2002).

⁸T. E. Oliphant, A. Manduca, R. L. Ehman, and J. F. Greenleaf, "Complex valued stiffness reconstruction for magnetic resonance elastography by algebraic inversion of the differential equation," *Magn. Reson. Med.* **45**, 299–310 (2001).

⁹M. Sridhar, H. Du, C. Pellot-Barakat, S. I. Simon, and M. F. Insana, "Ultrasonic mechanical relaxation imaging," *Proc. SPIE* **5373**, 202 (2004).

¹⁰E. E. W. Van Houten, J. B. Weaver, M. I. Miga, F. E. Kennedy, and K. D. Paulsen, "Elasticity reconstruction from experimental MR displacement data: Initial experience with an overlapping subzone finite element inversion process," *Med. Phys.* **27**, 101–107 (2000).

¹¹H. L. Oestrecher, "Field and impedance of an oscillating sphere in a viscoelastic medium with an application to biophysics," *J. Acoust. Soc. Am.* **23**, 707–714 (1951).

¹²T. J. Royston, Y. Yazicioglu, and F. Loth, "Surface response of a viscoelastic medium to subsurface acoustic sources with application to medical diagnosis," *J. Acoust. Soc. Am.* **113**, 1109–1121 (2003).

¹³A. Bot, R. H. W. Wientjes, and K. H. de Haas, "The transition zone for gelatin gels as measured by high-frequency rheology," *Imaging Sci. J.* **45**, 191–196 (1997).

¹⁴I. R. Titzte, S. A. Klemuk, and S. Gray, "Methodology for rheological testing of engineered biomaterials at low audio frequencies," *J. Acoust. Soc. Am.* **154**, 392–401 (2004).

¹⁵L. Sandrin, S. Catheline, M. Tanter, X. Hennequin, and M. Fink, "Time resolved pulsed elastography with ultrafast ultrasonic imaging," *Ultrason. Imaging* **21**, 259–272 (1999).

¹⁶J. Bercoff, S. Chaffai, M. Tanter, L. Sandrin, S. Catheline, M. Fink, J.-L. Gennisson, and M. Meunier, "In vivo breast tumor detection using transient elastography," *Ultrasound Med. Biol.* **29**, 1387–1396 (2003).

- ¹⁷W. F. Walker and G. E. Trahey, "A fundamental limit on the performance of correlation based on phase correction and flow estimation technique," *IEEE Trans. Ultrason. Ferroelectr. Freq. Control* **41**, 644–654 (1994).
- ¹⁸U. Hamhaber, F. A. Grieshaber, J. H. Nagel, and U. Klose, "Comparison of quantitative shear wave MR-elastography with mechanical compression tests," *Magn. Reson. Med.* **49**, 71–77 (2003).
- ¹⁹M. Djabourov, J. Leblond, and P. Papon, "Gelation of aqueous gelatin solutions. II. Rheology of the sol-gel transition," *J. Phys. (France)* **49**, 333–343 (1988).
- ²⁰L. Landau, E. Lifchitz, *Théorie de l'élasticité* (Mir, Moscou, 1990), Vol. 7, Chap. 5, Sec. 33.
- ²¹D. Royer and E. Dieulesaint, *Ondes Élastiques dans les Solides* (Masson, Paris, 1996), Vol. 1, Sec. 426.
- ²²J. L. Gennisson, S. Catheline, S. Chaffai, and M. Fink, "Transient elastography in anisotropic medium: Application to the measurement of slow and fast shear waves velocities in muscles," *J. Acoust. Soc. Am.* **114**, 536–541 (2003).
- ²³I. Sack, J. Bernarding, and J. Braun, "Analysis of wave pattern in MR elastography of skeletal muscle using coupled harmonic oscillator simulations," *J. Magn. Reson Imaging* **20**, 95–104 (2002).
- ²⁴E. L. Madsen, H. J. Sathoff, and J. A. Zagzebski, "Ultrasonic shear wave properties of soft tissues and tissuelike materials," *J. Acoust. Soc. Am.* **74**, 1346–1354 (1983).
- ²⁵L. Sandrin, M. Tanter, J.-L. Gennisson, S. Catheline, and M. Fink, "Shear elasticity probe for soft tissues with 1D transient elastography," *IEEE Trans. Ultrason. Ferroelectr. Freq. Control* **49**, 436–446 (2002).
- ²⁶S. Catheline, L. Sandrin, J.-L. Gennisson, M. Tanter, and M. Fink, "Ultrasound-based noninvasive shear elasticity probe for soft tissues," *IEEE Ultrasonic Symp.* **2**, 1799–1801 (2000).
- ²⁷L. Sandrin, B. Fourquet, J.-M. Hasquenoph, S. Yon, C. Fournier, F. Mal, C. Christidis, M. Ziol, B. Poulet, F. Kazemi, M. Beaugrand, and R. Palau, "Transient elastography: A new noninvasive method for assessment of hepatic fibrosis," *Ultrasound Med. Biol.* **29**, 1705–1703 (2003).
- ²⁸S. Catheline, J. L. Thomas, F. Wu, and M. Fink, "Diffraction field of a low frequency vibrator in soft tissues using transient elastography," *IEEE Trans. Ultrason. Ferroelectr. Freq. Control* **46**, 1013–1019 (1999).
- ²⁹D. C. Gakenheimer and J. Miklowitz, "Transient excitation of an half space by a point load traveling on the surface," *J. Appl. Mech.* **36**, 505–514 (1969).
- ³⁰H. Lamb, "On the propagation of tremors over the surface of an elastic solid," *Philos. Trans. R. Soc. London* **203**, 1–42 (1904).
- ³¹J.-L. Gennisson, "The 1D shear elasticity probe: A new tool to study biological tissues," thesis manuscript (in French), Paris VI University, France, 2003, Chap. 5, Sec. I.b.
- ³²R. Righetti, J. Ophir, S. Srinivasan, and T. Kroutskop, "The feasibility of using elastography for imaging the Poisson's ratio in porous media," *Ultrasound Med. Biol.* **30**, 215–228 (2004).
- ³³R. Sinkus, M. Tanter, T. Nisius, and C. Kuhl, "Anisotropic properties of breast cancer. *In Vivo* results utilizing a cubic model," Second International Conference on the Ultrasonic measurement and Imaging of Tissue Elasticity, Corpus Christi, TX, October 2003.